



Swansea University
Prifysgol Abertawe



Cronfa - Swansea University Open Access Repository

This is an author produced version of a paper published in :

Electrochimica Acta

Cronfa URL for this paper:

<http://cronfa.swan.ac.uk/Record/cronfa26340>

Paper:

Wint, N., de Vooy, A. & McMurray, H. (2016). The corrosion of chromium based coatings for packaging steel.

Electrochimica Acta

<http://dx.doi.org/10.1016/j.electacta.2016.01.100>

This article is brought to you by Swansea University. Any person downloading material is agreeing to abide by the terms of the repository licence. Authors are personally responsible for adhering to publisher restrictions or conditions. When uploading content they are required to comply with their publisher agreement and the SHERPA RoMEO database to judge whether or not it is copyright safe to add this version of the paper to this repository.

<http://www.swansea.ac.uk/iss/researchsupport/cronfa-support/>

Accepted Manuscript

Title: The corrosion of chromium based coatings for packaging steel

Author: N. Wint A.C.A. de Vooy H.N. McMurray

PII: S0013-4686(16)30101-3
DOI: <http://dx.doi.org/doi:10.1016/j.electacta.2016.01.100>
Reference: EA 26482

To appear in: *Electrochimica Acta*

Received date: 28-8-2015
Revised date: 12-1-2016
Accepted date: 14-1-2016

Please cite this article as: N.Wint, A.C.A.de Vooy, H.N.McMurray, The corrosion of chromium based coatings for packaging steel, *Electrochimica Acta* <http://dx.doi.org/10.1016/j.electacta.2016.01.100>

This is a PDF file of an unedited manuscript that has been accepted for publication. As a service to our customers we are providing this early version of the manuscript. The manuscript will undergo copyediting, typesetting, and review of the resulting proof before it is published in its final form. Please note that during the production process errors may be discovered which could affect the content, and all legal disclaimers that apply to the journal pertain.



The corrosion of chromium based coatings for packaging steel

N.Wint*¹, A.C.A. de Voos², H. N. McMurray¹,

¹ *Materials Research Centre, College of Engineering, Swansea University, Bay Campus,*

Fabian Way, Crymlyn Burrow, Swansea, UK, SA1 8EN

² *Tata Steel, P.O. Box 10.000, 1970 CA IJmuiden, The Netherlands*

***Corresponding author:** Tel: +44 7989676416

Email: 483404@swansea.ac.uk

Abstract

Chromium/chromium oxide based coatings, cathodically electrodeposited from either Cr (VI) or Cr (III) containing electrolytes are compared with respect to their ability to resist the corrosion driven delamination of an adherent polymer overcoat. Cathodic disbondment rates are determined using an in-situ scanning Kelvin probe technique. Anodic disbondment (filiform corrosion, FFC) rates are determined optically. The Cr (VI) derived coatings were fully resistant to corrosion driven disbondment. The Cr (III) derived coatings exhibited measurable rates of both FFC and cathodic disbondment. Disbondment kinetics are explained in relation to coating morphology, porosity and chemical composition determined using a combination of scanning electron microscopy (SEM), transmission electron microscopy (TEM) and xray photoelectron spectroscopy (XPS).

Keywords: Chromium; Packaging; Organic coatings; Steel; Atmospheric corrosion.

1 Introduction

Hexavalent chromium based electrolyte baths are traditionally used during the production of coatings for packaging steel, primarily electro chromium coated steel (ECCS), or tin free steel (TFS). The material consists of a thin gauge (0.13-0.49 mm) low carbon steel substrate with a thin coating, comprising of a base layer of chromium metal and a top layer of chromium oxide, produced using chromic acid.

There is significant current interest in the development of chromium free coatings due to the international concern regarding environmental health [1, 2, 3, 4, 5]. Alternatives should be equivalent or better than existing treatments, non-toxic, acceptable to the food industry, and capable of application under similar tinning line conditions [6]. One approach to doing this has been the application of the chromium/chromium oxide coating from a trivalent (III) chromium salt based electrolyte [5, 7].

The principal purpose of the coating on packaging materials is to provide corrosion resistance. In the case of ECCS iron, exposed during can forming, has previously been found to act as an initiation site for corrosion [8]. The material is therefore used in conjunction with an organic (lacquer or laminate) overcoat. Two mechanisms of corrosion are of primary concern; firstly, wet corrosion where the internal packaging surface is in contact with the contents [9] and secondly, atmospheric corrosion of the external surface.

The aim of the current paper is to present a detailed study of the role of technologically important chromium based coatings in resisting corrosion driven coating delamination that occurs at penetrative defects in these organic coatings. Firstly, the well understood cathodic disbondment mechanism, during which the delamination of the organic coating from the metal substrate is driven by the cathodic reaction (usually oxygen reduction), is studied. Within the localised corrosion cell, anodic metal dissolution located in the vicinity of the

defect is coupled to the cathodic delamination front by a thin ($<5\mu\text{m}$) gel like electrolyte, which ingresses beneath the coating [10]. Secondly anodic delamination, or filiform corrosion (FFC), which produces ‘threadlike’ corrosion product deposits, whereby failure is often linked to an anodic reaction [10]. It is widely accepted that filament advance involves anodic undercutting at the ‘active head’, driven by differential aeration arising from facile O_2 diffusion in the filament tail, which consists of dry corrosion products [10, 11, 12, 13, 14, 15].

Although passivation systems based on titanium [9] and zirconium [16] have previously been investigated on tinplate, they were found to be poor in terms of performance and often require different application technologies. Trivalent chromium based coatings have been found to perform effectively on both aluminium and zinc [17, 18]. When directly comparing trivalent and hexavalent chromium based conversion coatings using polarisation data, Zhang et. al found that Cr(III) based baths inhibited the corrosion of zinc to a significant degree, but less effectively than the coating produced using a Cr(VI) bath. The difference was attributed to the thinner layer produced in the case of Cr(III) based coatings [19].

During the work described here steel, used in conjunction with both trivalent and hexavalent chromium based systems (ECCS), are organically coated using a model polyvinyl butyral organic lacquer, and their resistance to corrosion driven organic coating delamination, by both anodic and cathodic mechanisms, are investigated. Corrosion driven cathodic delamination is investigated by employing a ‘Stratmann’ type cell, and a $0.86\text{ mol}\cdot\text{dm}^{-3}$ aqueous sodium chloride (NaCl) electrolyte is used to reflect standard accelerated corrosion test conditions [20, 21]. The time dependent extent of cathodic disbondment is determined by repeated in situ scanning using a scanning Kelvin probe (SKP) apparatus. The capability of the SKP to visualise the spatial distribution of localised free corrosion potential variation with time has been demonstrated previously [20, 21]. Anodic disbondment (FFC) is initiated using

FeCl₂ and the time dependent extent of corrosion is determined optically. Results are explained in relation to coating morphology, porosity and chemical composition determined using a combination of scanning electron microscopy (SEM), transmission electron microscopy (TEM) and xray photoelectron spectroscopy (XPS). In doing this we hope to determine the viability of using trivalent chromium based coating systems, which make use of the same application technology as for current sodium dichromate passivation systems, as alternatives to those produced using hexavalent chromium.

2 Experimental

2.1 Materials

Iron foil of 0.15mm thickness and 99.5% purity was obtained from Goodfellow Cambridge Ltd. Low alloy mild strip steel of 0.2 mm gauge, with two different types of coatings applied, were obtained from Tata Steel Packaging. In the case of the first material the chromium-chromium oxide layer was applied to the cathodic steel strip from a hexavalent chromium based chromic acid electrolyte. This product is referred to as ECCS. In the case of the second material the coating was applied from a trivalent chromium salt based electrolyte using a process described elsewhere [7].

Polyvinyl butyral (PVB) and all other chemicals were obtained from Aldrich Chemical Co. and of analytical grade purity.

2.2 Methods

2.2.1 Materials Characterisation

X-ray Photoelectron Spectroscopy (XPS) spectra and depth profiles were recorded on a Kratos Axis Ultra using Mg Ka x-rays of 1253.6 eV. The measured spot size was 700 mm ×

300 mm. The depth profiles were recorded using 4 keV Ar⁺ ions creating a sputter crater of 3 mm × 3 mm. The composition was determined by fitting the XPS spectra of the Cr2p, O1s and C1s peak. The latter two were used to refine the quantification of the oxide and carbide content [5]. Determination of the individual Cr-species from the XPS spectra, Figure 1, was performed using the following procedure. Peaks from metallic chromium and chromium carbides overlap. The carbide part of the C1s peak was well separated from other species within the peak and can therefore be quantified reliably. The amount of chromium carbide present was thus calculated, assuming it existed in the form Cr₃C₂.

(Figure 1)

The overall Cr weight, determined by integrating over the entire depth, was ca. 60 mg.m⁻² (25.1 mg.m⁻² metallic chromium, 16.1 mg.m⁻² chromium oxide and 18.8 mg.m⁻² chromium carbide). In comparison, in the case of ECCS, the overall Cr weight was ca. 80 mg.m⁻² (69 mg.m⁻² metallic chromium, 8 mg.m⁻² chromium oxide and 3 mg.m⁻² chromium carbide).

Scanning electron microscopy (SEM) images were collected using a Zeiss Ultra 55 with an InLens detector. Representative locations were found using light imaging microscopy (LIM) and SEM, and were selected for cross sectioning. Cross sections were prepared using a focused ion beam (FIB), before which they were ultrasonically cleaned in isopropanol for 10 minutes. The samples were coated with a thin (30nm) pure metallic platinum (Pt) layer via sputter coating. A platinum layer was deposited by dissociation of a volatile organic Pt complex using an electron beam (which does not affect the sample). The organic Pt complex was dissociated using a Ga ion beam (where the sample is protected by the first two layers). The first Pt layer is easily recognised in the TEM and marks the original surface; subsequent layers contain more carbon and are thus less bright in the TEM images. The final thinning stage was performed on a Nova Nanolab200 Small Dual Beam.

Transmission electron microscopy (TEM) imaging and analysis was performed using a FEI Tecnai F30ST, operating at 300kV, and equipped with a Field Emission Gun (FEG) and an energy dispersive x-ray spectrometer (EDX) spectrometer. The TEM was also equipped with a high angle annular dark field (HAADF) detector. The contrast in HAADF images is well resolved by atomic number (Z). Contrast in composition shown in images is thus similar to that obtained using the back scattered detector in an SEM.

2.2.2 Electrochemical Characterisation

Direct current electrochemical experiments were conducted using a Solartron 1280 Electrochemical Measurement Unit. A saturated calomel electrode (SCE) reference electrode was used to provide a fixed potential throughout the experiment. Coupons of approximately 40 mm x 30 mm were cut from large sheets to obtain a suitably sized sample. The sample was masked using extruded polytetrafluoroethylene (PTFE) tape (type 5490 HD supplied by 3M) which exposed a 10 mm x 10 mm area in the centre. Materials were characterised in terms of their open circuit potential (OCP) at 20°C in a 0.1 M HCl electrolyte. The primary intention of taking potential measurements in acid was to determine the likely galvanic series for iron and chromium based coatings in an electrolyte relevant to the anterior portion of the FFC head [11, 12]. This was done to determine whether or not a coating would anodically dissolve when coupled to the iron substrate. Potentiodynamic scans were conducted in an aerated 0.6 mol.dm⁻³ NaCl electrolyte at 20°C. The primary intention of potentiodynamic polarisation experiments was to characterise cathodic activity for oxygen reduction on various substrates. This is directly relevant to cathodic disbondment [21], and indirectly relevant to FFC (where the coating maybe partly or wholly removed by anodic dissolution), by showing whether residual coating or substrate iron will present the most active site for

oxygen reduction. A platinum gauze counter electrode and a scan rate of $0.1667 \text{ mV}\cdot\text{sec}^{-1}$ were used. Three repeat measurements were made.

Prior to corrosion studies the materials were cut into coupons of 5 cm x 5 cm. In the case of the pure iron the surface was lightly abraded. All samples were cleaned and degreased before experimentation. All samples were solvent coated with 15% w/w ethanolic solution of polyvinyl butyral (PVB), molecular weight 70,000-100,000, lacquer using insulating tape height guides to give an air-dried thickness of 30 μm , as determined using a micrometer screw gauge.

For cathodic delamination experiments, coatings were partially peeled back to create a defect comprising a 20 x 15 mm area of bare metal. A residual lip of clear adhesive tape and overcoated PVB formed a barrier between the intact polymer coated metal surface and the electrolyte applied to the defect area. Non corrosive silicone rubber was applied to the remaining edges of the defect to form a reservoir sufficient to contain a 2 cm^3 volume of corrosive electrolyte. When conducting cathodic delamination experiments humidity was kept constant at 95% RH by use of electrolyte reservoirs containing $0.86 \text{ mol}\cdot\text{dm}^{-3}$ aqueous NaCl at pH 6.5 in the chamber. Experiments took place at room temperature. An aliquot of electrolyte was applied to the defect to initiate the delamination. The reference probe was moved over the surface along a 12mm line up to the boundary of the defect. Measurements were therefore made approaching the defect ($\sim 100\mu\text{m}$ away at closest approach). The SKP chamber was closed and scans taken at regular intervals after initiation. Scans were recorded as a numeric grid on the computer. In the case of deaerated cathodic delamination experiments, corrosion was allowed to initiate in the presence of oxygen before nitrogen was sparged through the $0.86 \text{ mol}\cdot\text{dm}^{-3}$ NaCl electrolyte, prior to entering the chamber. Full details of the SKP apparatus and calibration have been described elsewhere [22, 23]. Three repeat measurements were taken for each material.

In the case of FFC two types of sample were prepared. In the case of the first type the chromium coated surface was continuous. In the case of the second type the chromium based coating was removed from half the sample surface. Two types of experiment were carried out. In the first type FFC was initiated on the coating. In the second type FFC was initiated on the exposed steel substrate and allowed to propagate over the coated portion of the sample. All samples were solvent coated with 15% w/w ethanolic solution of polyvinyl butyral (PVB). A 10 mm line penetrative PVB coating defect was created by scribing the sample with a scalpel blade. FFC was initiated by introducing 2 μL of 2.5×10^{-3} M aqueous FeCl_2 evenly over the length of the scribe using a glass microcapillary, following a procedure described elsewhere [24]. After allowing the FeCl_2 to react with the exposed metal, and excess water to evaporate in air, samples were placed in an environmental chamber. The temperature was constant at 20°C and a relative humidity of 93% RH was maintained throughout the experiment by allowing the atmosphere to remain in equilibrium with a reference solution comprising saturated aqueous $\text{Na}_2\text{SO}_4 \cdot 10\text{H}_2\text{O}$. Samples were removed from the humidity chamber at intervals in time to carry out photography and computerised image analysis. The image analysis software (Sigma Scan Pro) was calibrated by specifying a pre-measured distance between two points and inputting real distance. The surface area of the FFC attack was measured as that occupied by corrosive discolouration. A value for a designated surface area was then given. SEM images showing FFC morphology were obtained using a Hitachi tabletop microscope TM3000.

3 Results

3.1 Material characterisation

The SEM images at lower magnification (first three images in Figure 2) show that the substrate steel is heterogeneous (varying rolling roughness, traces of contaminations, etc.).

The grain boundaries of the steel substrate are easily identified and other origins for heterogeneity can also be discerned. At higher magnification (1 μm) the SEM images show that the coating follows the structure of the steel substrate and is applied homogeneously on each steel grain. The grains of the Cr coating are in the 10-20 nm range. The SEM images at the highest magnification show the presence of circular features (indicated by arrows) with a diameter of *ca.* 50-100 nm. During the chromium deposition process 90% of current is attributed to the evolution of hydrogen [5]. It is therefore proposed that the presence of these circular features results from the attachment of gas bubbles to the surface. At these positions the deposition process will be hindered compared to the rest of the surface and thus a circular feature will be present.

It is worth noting that a similar chromium grain structure is seen in the SEM image of ECCS (Figure 2ii) at a similar magnification. ECCS also exhibits heterogeneities, as with any material produced on an industrial scale [25]. Hydrogen evolution is suggested to occur at sites at which 'circles' are present. However, in comparison to Cr^{3+} based coatings, Cr^{6+} ions will spontaneously deposit onto most surfaces (including carbon-containing species), providing additional corrosion inhibition.

(Figure 2)

The resolution associated with SEM images is not high enough to discern changes in composition of the Cr grains. The coating layer is also too thin to image in cross section. Both pieces of information are required to interpret XPS depth profiles, which are averaged over the entire spot. Samples were therefore coated with a protective platinum layer (which also acts to mark the original outer sample surface), cross sectioned with FIB, and analysed using a TEM. The results are given in Figure 3 and Figure 4. Dark lines \sim 5-20 nm apart, and perpendicular to the surface, can be seen in the enlarged image of the TEM cross section

shown in Figure 4i. The distance between the lines relates to the size of the Cr grains in the SEM images and it is thus proposed that they correspond to grain boundaries of the Cr coating. The HAADF detector is sensitive to both the elemental composition (a higher atomic number will show brighter in the image) and to the density (a higher density will give a brighter image). As an EDX line scan showed no difference in elemental composition, the difference in colour can be attributed to a slight decrease in density rather than the presence of lighter elements. A decrease in density is typical for a grain boundary; i.e., the layer is closed on the nm scale. The cross section also shows a position where the steel substrate is uneven, due to a crevice caused by the rolling roughness (Figure 4ii). The Cr coating is deposited preferentially into the crevice (yellow triangle), with only a small void at the tip, which is suggested to occur due to the electrolyte resistance.

(Figure 3 and Figure 4)

Given the number and random scattering of the circles observed in the SEM images, it is highly likely that one of them is cut in the TEM cross section shown in Figure 3 and Figure 4. It is of importance that it is determined whether the circles are topological or permeating in nature. In the latter case the steel substrate will be exposed, this being detrimental in terms of corrosion resistance. As there is no evidence of holes permeating through the surface, or of protrusions associated with the “rim” around a circle, it is inferred that the circular features, suggested to represent hydrogen bubbles, are superficial in nature.

The XPS depth profiles are given in Figure 5. The outer surface of the Cr³⁺ coating is enriched in oxide, but the layer itself is a mixture of Cr-metal, Cr-oxide and Cr-carbide. A significant amount of Fe is detected in the layer. It is postulated that this is due to porosity in the Cr layer (the XPS spot size was 700x300 μm, and the SEM images show some porosity on that scale). In comparison the XPS profiles obtained in the case of ECCS show a higher

amount of Cr-OH groups at the outer surface of the coating compared to the Cr³⁺ based coating, this being related to the two-stage process where the second deposition step deposits solely oxides [5].

(Figure 5)

OCP Characterisation Results

All materials were characterised in terms of their OCP at 20°C in a 0.1 M HCl electrolyte, the results being shown in Table I. The confidence limits (errors) shown correspond to ± one unit of standard deviation on the mean, on the basis of three repeat measurements. The values obtained are, within experimental error, identical for all materials. The galvanic polarity of a cell formed between the iron substrate and the chromium based coatings can therefore not be inferred. It is suggested that in the case of porous, or imperfect, coatings the exposed iron will dominate the potential reading.

(Table I)

Potentiodynamic Results

Potentiodynamic scans were conducted in a 0.6 mol.dm⁻³ NaCl electrolyte at 20°C. A scan rate of 0.1667 mV.sec⁻¹ was used and results are shown in Figure 6. Figure 6 shows that cathodic currents measured on ECCS are significantly smaller (~100 times) than those observed for pure iron and Cr³⁺ based coatings on steel. Anodic current values are highly dependent on polarisation potential, however at a potential value of ~0V vs. SHE (standard hydrogen electrode) the current measured for ECCS, is over ten times smaller than that for both pure iron and Cr³⁺ based coating systems. The three zero current measurements observed in the case of iron indicates an active/passive transition suggesting the material is unstable, this being expected at the relevant pH [26].

(Figure 6)

3.2 Resistance to organic coating failure by cathodic disbondment

The kinetics of disbondment of the PVB lacquer from pure iron was determined in an initial experiment to establish baseline characteristics in the absence of a chromium coating. After initiation the time dependent $E_{corr}(x)$ profiles (where x is distance from the defect edge) became established, and are shown in Figure 7. E_{corr} values over the intact coating surface (E_{intact}) were uniformly high and remained constant at *ca.* 0.2 V vs. SHE, this being similar to those reported previously [27]. E_{corr} values in the vicinity of the delamination front fall to match that of the bare metal in contact with electrolyte in the defect, in this case *ca.* -0.3 V vs. SHE, this being expected for anodically active iron (*ca.* -0.44 V vs. SHE) [20, 21, 28, 29]. It has been shown that during coating delamination a local cathode, resulting from the oxygen reduction reaction (ORR), exists in the region of the delamination front resulting in loss of coating adhesion. Anodic iron dissolution is constrained to the vicinity of the coating defect [21]. The anodic and cathodic reactions are linked by the ionic transport of current through the underfilm electrolyte. Throughout the duration of the experiment the electrolyte ingresses further under the coating. The linear gradient in potential between E_{corr} at the delamination front and undelaminated region is the result of the ionic conductivity in the underfilm electrolyte. The point of maximum gradient in time dependent $E_{corr}(x)$ profiles has been identified as a semi-empirical means of locating the cathodic delamination front [21, 22, 27]. As delamination time increases the linear gradient moves further away from the defect. The rate of this progression decreases with time. This is indicative of the delamination rate being controlled by the migration of electrolyte cations (here Na^+) from external (defect zone) electrolyte to the cathodic delamination front [27, 28]. Under these circumstances the distance (x_{del}) over which delamination has occurred is related to the time since electrolyte

contact (t_{del}) by equation (1), where k_d is the delamination rate constant and t_i the initiation period.

$$x_{del} = k_d (t_{del} - t_i)^{1/2} \quad (1)$$

Figure 8 shows plots of x_{del} vs. $(t_{del} - t_i)^{1/2}$ obtained from time dependent E_{corr} profiles for iron. The curve is a good straight line consistent with migration control and thus parabolic kinetics. The k_d value obtained from the gradient was $(550 \pm 79) \mu\text{m}\cdot\text{min}^{-1/2}$. The confidence limits (errors) shown correspond to \pm one unit of standard deviation on the mean. Error bars are omitted for the sake of clarity.

(Figure 7 and Figure 8)

Cathodic driven coating delamination was not observed on ECCS over a time period of 96 hours, for three repeat measurements, this being made evident by the potential plateau shown in Figure 9. In the case that delamination does not occur there is no coupling to the defect and therefore $E_{corr} \gg$ than that for the bare metal in contact with the electrolyte.

(Figure 9)

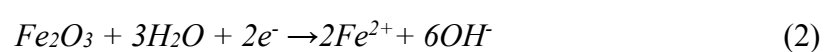
In comparison, cathodic disbondment was observed on Cr^{3+} based coatings. Figure 10 shows $E_{corr}(x)$ profiles that are separated by a constant distance as time progresses. This suggests the system is controlled by linear kinetics which are produced when the rate is controlled by electron transfer. The delamination rate constant was calculated as $(7.7 \pm 2.3) \mu\text{m}\cdot\text{min}^{-1}$ from Figure 11. It is suggested that delamination may be observed in the case of Cr^{3+} coatings, and not ECCS, due to the increased exposed iron substrate and the presence of metallic iron at the outer surface of the coating. As shown in Figure 6, larger cathodic currents are observed for pure iron than Cr^{3+} coated steel, and thus cathodic delamination will progress at a faster rate in the presence of iron.

(Figure 10 and Figure 11)

The change in kinetics from parabolic to linear, with the introduction of a Cr^{3+} coating, can be confirmed by use of a different electrolyte. Stratmann et al. found that a linear relationship exists between delamination area and square root of time, this proving that diffusion of cations from the anode to the cathode is a rate determining step for systems displaying parabolic kinetics [28]. It was also concluded that the smaller the cation size the slower the rate, this corresponding to the dependence on diffusion coefficient in aqueous electrolytes [28]. The rate will not, however, be influenced in a system that exhibits linear kinetics. The electrolyte cation was therefore changed from sodium to caesium. As can be seen in Figure 12 the rate is within experimental error, similar, in the case of both NaCl, for which a delamination rate of $(4.5 \pm 1.35) \mu\text{m min}^{-1}$ was obtained and CsCl, for which a rate of $(3.1 \pm 0.9) \mu\text{m min}^{-1}$ was obtained.

(Figure 12)

Cathodic delamination was then studied in the absence of oxygen. This is especially important when considering both the low oxygen partial pressure in a food can environment and the autoreduction reaction, given by equation (2), which occurs as a result of the ability of iron to exist in more than one oxidation state [30].



The reduction of Fe^{3+} can thus drive oxidation at the defect, and consequently cathodic delamination can proceed in the absence of oxygen.

Delamination was allowed to initiate in the presence of oxygen before nitrogen was sparged through the 0.86 mol.dm^{-3} sodium electrolyte prior to entering the chamber. Alongside this experiment another was conducted during which the SKP was used to scan a sample, half of

which consisted of the exposed blackplate substrate, the other half where the coating was intact. A line scan was taken across the sample both in the presence and absence of oxygen. The change in the potential when the atmosphere within the Kelvin probe chamber is changed from that containing oxygen to solely inert nitrogen, has previously been used as an indication of the ability of a material to reduce oxygen [31].

A potential drop is observed at the defect, due to a reduction in the rate of the cathodic partial reaction when nitrogen is introduced [30], as shown in Figure 13. The presence of an equipotential region within the delaminated zone, in the absence of oxygen, has been noted elsewhere [30]. In this case the presence of the chromium/chromium oxide layer results in zero ionic transport, and thus a potential gradient does not exist when the oxygen reduction reaction rate decreases. Figure 14 shows that the rate of delamination decreases, to 0.15 that of the original, in the absence of oxygen.

(Figure 13 and Figure 14)

Both this reduction in delamination rate and the finding that potential value is independent of atmosphere, as shown in Figure 15, suggests that the Cr^{3+} layer does not support autoreduction.

(Figure 15)

Although there is a lower oxidation state, Cr^{2+} , the reduction of Cr^{3+} to Cr^{2+} given by equations (3) and (4) is unable to support the oxidation of Fe^0 to Fe^{2+} (6) at a pH typical of those within the delaminated region (pH10-12) [28]. Reaction (5) was not considered as a viable reaction as chromic hydroxide, $\text{Cr}(\text{OH})_3 \cdot n\text{H}_2\text{O}$, has a very limited range of stability between approximately pH 8 and 9 [26].

$$E = -0.785 - 0.0591\text{pH} \qquad E \text{ (V vs. SHE)} = -1.376 \text{ V (pH 10)} \qquad (3)$$

$$E = -0.561 - 0.0591pH \quad E (V \text{ vs. SHE}) = -1.152 V (pH 10) \quad (4)$$

$$E = -0.360 - 0.0591pH \quad E (V \text{ vs. SHE}) = -0.951 V (pH 10) \quad (5)$$

$$E = -0.440 + 0.0295 \log (Fe^{2+}) \quad E (V \text{ vs. SHE}) = -0.440 V (1M) \quad (6)$$

It is thus suggested that autoreduction occurs at iron exposed by pores in the coating, this leading to the continuation of delamination, albeit at a reduced rate. This notion is supported by the presence of a small local reduction in potential, shown in Figure 13, at the delamination front, at which autoreduction would typically occur. It is also possible that autoreduction is able to occur as a result of the metallic iron present in the chromium layer as shown in Figure 5. This proposal is supported by Figure 6 which shows significantly increased cathodic currents for Cr^{3+} coated systems, in comparison to ECCS. It is suggested that the increased currents measured in the case of the former material is the result of iron from the substrate ‘doping’ the coating during production.

3.3 Resistance to organic coating failure by anodic disbondment (FFC)

It is widely accepted that filament advance involves anodic undercutting at the ‘active head’. This process is driven by differential aeration arising from facile O_2 diffusion in the filament tail, which consists of dry corrosion products [10, 11, 12, 32]. Elsewhere it has been suggested that delamination of the protective layer from the substrate is due to cathodic mechanisms in the vicinity of the head [33]. Williams and McMurray observed an area of cathodic delamination but contest its function as a primary cathode, claiming it plays no role in the mechanism of FFC advance [24].

Figure 16 shows that FFC could not be initiated on ECCS using a 0.0025 M $FeCl_2$ electrolyte. The similarity of the images taken ii.) three weeks and iii.) five weeks after initiation on the steel substrate demonstrate that FFC could not propagate onto the ECCS

coated steel. The open circuit potential measurement taken in 0.1 M HCl electrolyte (pH 1) for Cr³⁺ coatings is, within experimental error, identical to that recorded for pure iron and therefore the protection mechanism cannot be inferred. It is however suggested that the chromium/chromium oxide based coating retards the anodic reaction rate, a cathode having already been established on the steel substrate. The depth of FFC into steel has previously been reported as up to 10 µm, this being substantially more than the thickness of the chromium/chromium oxide layer (~50nm) [12]. It is subsequently proposed that had the coating not acted to retard the anodic reaction it would have been destroyed and thus the substrate would have been exposed allowing FFC propagation to continue.

(Figure 16)

In comparison, Figure 17 shows that FFC was both i.) initiated and ii.) propagated onto Cr³⁺ coated steel. The SEM image in Figure 18 suggests that filament advance is salutatory in nature, where propagation exists in a step-wise or discrete manner [34]. The constant propagation rate is indicative that there is no mass transport limitation and that the facile diffusion of oxygen through the dry corrosion products within the filament tail has negligible effect on rate of extension [34]. In the bottom left of Figure 18 a build-up of corrosion product is evident, this being indicative of the coating being damaged and that substrate corrosion has occurred. It should be considered that more corrosion product may be present if it were not for removal of the PVB lacquer prior to image acquisition.

There are two possible explanations for the protection offered by the chromium/ chromium oxide derived coatings based on their chemical composition. The first considers the metallic chromium content of the layers. As explained, coatings produced using hexavalent chromium contain over double the amount of metallic chromium as those derived from trivalent chromium. It may therefore be suggested that ECCS exhibits a superior resistance to both

cathodic delamination and filiform corrosion due to the higher metallic chromium compared to Cr^{3+} based coatings. However chromium does not display passivity at low pH [26], typical of those within the FFC head electrolyte [11, 12]. It is thus suggested that the chromium oxide provides a partial barrier to the anodic reaction and that corrosion rate is thus dependent on coating uniformity and defect population.

(Figure 17 and Figure 18)

4.0 Discussion

The difference in corrosion resistance of the coatings may exist due to a number of factors. It is believed that Cr^{3+} based coatings, SEM images of which are shown in Figure 2, are relatively imperfect (with penetrative defects) when compared to the Cr^{6+} based coating produced in the case of ECCS. This is particularly apparent at heterogeneities in the coating that are visible on the larger scale (above 1-10 μm spacing), for example due to varying rolling roughness and at sites of contamination. The activity of Cr^{6+} during plating means that it is reduced to Cr^{3+} rapidly when in contact with iron, which is considered to be relatively noble. Consequently very little iron is exposed in the case of undeformed ECCS. In comparison Cr^{3+} based coatings are deposited due to a local change in pH at the substrate surface which occurs as a result of the hydrogen evolution reaction [5, 7]. The lack of spontaneous deposition at heterogeneities provides a higher porosity. It is believed that this, alongside iron ‘doping’ of the coating leads to increased cathodic currents and thus cathodic delamination rates. In the case of FFC it is suggested that the chromium oxide provides a partial barrier to the anodic reaction and that the corrosion rate is thus dependent on coating uniformity and defect population.

The chemical nature of the outer surface, particularly the availability of Cr-OH groups, plays a key role in the adhesion, which is defined as an important property of a coating [10].

However, improving coating adhesion alone may not improve resistance to cathodic delamination and FFC if an alternative disbondment mechanism, such as hydrolysis, is available [35]. Irrespective, the possible influence of Cr-OH group population should be considered during comparison of coating resistance to corrosion driven coating disbondment. The XPS profiles show a higher amount of Cr-OH groups at the outer surface of the ECCS coating than the Cr³⁺ based coating, this being related to the two-stage process where the second deposition step deposits solely oxides [5]. The TEM images also show that the Cr³⁺ based layer has a single chemical composition. In comparison, ECCS is composed of two layers (metallic Cr with a Cr-oxide on top). [8, 25] This may contribute to the increased resistance of ECCS to both cathodic delamination and FFC, together with other factors.

4 Conclusions

A comparison between coatings produced using hexavalent and trivalent chromium based electrolyte baths, with regards to their resistance to atmospheric corrosion, has been completed to show that;

- The Cr (VI) derived coatings were fully resistant to corrosion driven disbondment.
- On Cr³⁺ based coatings the rate of FFC was substantially reduced when compared to that measured on pure iron,
- Disbondment via the cathodic delamination mechanism was found to occur on trivalent chromium coatings,
- Disbondment via the cathodic delamination mechanism on trivalent chromium based coatings occurred at a significantly reduced rate in deaerated conditions, typical of those within packaging products.

It is proposed that;

- Differences between the Cr³⁺ and Cr⁶⁺ based coatings in terms of resistance to atmospheric corrosion, such as cathodic delamination and FFC occur, firstly due to pores in the Cr³⁺ coating which exist as a result of the deposition mechanism, and secondly due to the chemical composition of the coating. XPS depth profiles show that Cr³⁺ layers have higher levels of surface metallic iron and less outer OH⁻ groups, which may contribute to increased rates of corrosion driven coating delamination.
- Trivalent chromium based coatings for use on packaging steel may be a feasible alternative to traditional hexavalent based systems with respect to corrosion resistance, especially with a reduced porosity. This proposed alternative also makes use of the same application technology as for current passivation systems.
- It is suggested that future work concentrates on the quantitative measurement of the adhesion of organic coatings and lacquers to chromium based coatings, and consequently the correlation between adhesion and corrosion properties.

5. Acknowledgments

The authors would like to thank the European Social Fund (ESF) through the Welsh Government for the financial support of the Steel Training Research and Innovation Partnership (STRIP). In addition, the support from TATA Steel is gratefully acknowledged. Dr. K.R. Lammers is acknowledged for the FIB-TEM and XPS analysis, and Dr. M. Aarnts for the high resolution SEM images

References

- [1] N. Mora, E. Cano, J.M. Bastidas, E. Almeida, J. M. Puente, Characterization of passivated tinfoil for food can applications, *Journal of Coatings Technology*, 74 (2002) 53-58.
- [2] I.S. Rees, EUR 17860 Properties and in service performance; Development of chromium free passivation films for tin plate, Office for Official Publications of European Communities, Luxembourg, 1998.
- [3] S. A. Katz, H. Salem, The toxicology of chromium with respect to its chemical speciation: A review, *Journal of Applied Toxicology*, 13 (1993) 217-224.
- [4] S. Langård and T. Norseth, A cohort study of bronchial carcinomas in workers producing chromate pigments, *British Journal of Industrial Medicine*, 32 (1975) 62-65.
- [5] J.H.O.J. Wijenberg, M. Steegh, M. P. Aarnts, K. R. Lammers, J. M. C. Mol, Electrodeposition of mixed chromium metal-carbide-oxide coatings from a trivalent chromium-formate electrolyte without a buffering agent, *Electrochimica Acta*, 173 (2015) 819-826.
- [6] A. Sheffet, I. Thind, A. M. Miller, and D. B. Louria, Cancer mortality in a pigment plant utilizing lead and zinc chromates, *Archives of Environmental Health: An International Journal*, 37 (1982) 44-52.
- [7] J. H. O. J. Wijenberg, Tata Steel, Method for manufacturing chromium- chromium oxide coated substrates, Patent WO 2014/202316, 24 December 2014.

- [8] B. Boelen, H. den Hartog, H. van der Weijde, Product performance of polymer coated packaging steel, study of the mechanism of defect growth in cans, *Progress in Organic Coatings*, 50 (2004) 40-46.
- [9] E. Almeida, M. R. Costa, N. De Cristofaro, N. Mora, R. Catalá, J. M. Puente, J. M. Bastidas, Titanium passivated lacquered tinfoil cans in contact with foods, *Corrosion Engineering, Science and Technology*, 40 (2005) 158-164.
- [10] H. N. McMurray, G. Williams, 2.14 Underfilm/Coating Corrosion, in: T.A.J. Richardson (Ed.), *Corrosion in Liquids, Types of Corrosion in Liquids, Shreir's Corrosion*, vol 2, fourth ed., Elsevier Ltd., 2009, p.988.
- [11] A. Bautista, Filiform corrosion in polymer coated metals, *Progress in Organic Coatings*, 28 (1996) 49-58.
- [12] R. T. Ruggeri, and T. R. Beck, An analysis of mass transfer in filiform corrosion, *Corrosion-NACE*, 39 (1983) 452-465.
- [13] W. Schmidt, and M. Stratmann, Scanning Kelvin probe investigations of filiform corrosion on aluminium alloy 2024-T3, *Corrosion Science*, 40 (1998) 1441-1443.
- [14] G. Grundmeier, W. Schmidt, and M. Stratmann, Corrosion protection by organic coatings: electrochemical mechanism and novel methods of investigation, *Electrochimica Acta*, 45 (2000) 2515-2533.
- [15] J. H. W. de Wit, New knowledge on localized corrosion obtained from local measuring techniques, *Electrochimica Acta*, 46 (2001) 3641-3650.
- [16] L.S. Rees, Development of chromium free passivation films for tinfoil, 6th International Tinfoil Conference ITRI; London; 1996. pp. 291-296.

- [17] H. Bhatt, Trivalent chromium conversion coating for corrosion protection of aluminium surfaces, *Metal Finishing*, 107 (2009) 31-37.
- [18] K. Woo Cho, V. Shankar Rao, H. Kwon, Microstructure and electrochemical characterization of trivalent chromium based conversion coating on zinc, *Electrochimica Acta*, 52 (2007) 4449-4456.
- [19] X. Zhang, C. van de Bos, W. G. Sloof, A. Hovestad, H. Terryn, J. H. W. de Wit, Comparison of the morphology and corrosion performance of Cr (VI) and Cr (III) based conversion coatings on zinc, *Surface and Coatings Technology*, 199 (2005) 92-104.
- [20] M. Stratmann, H. Streckel, R. Feser, A new technique able to measure directly the delamination of organic polymer films, *Corrosion Science* 32 (1991) 467-470.
- [21] A. Leng, H. Streckel, M. Stratmann, The delamination of polymeric coatings from steel. Part 1: Calibration of the Kelvinprobe and basic delamination mechanism, *Corrosion Science*, 41 (1999) 547-578.
- [22] G. Williams, H.N. McMurray, Chromate inhibition of corrosion driven organic coating delamination studied using a scanning Kelvin probe technique, *Journal of the Electrochemical Society*, 148 (2001) B377-B385.
- [23] G. Williams, H. N. McMurray, D. A. Worsley, Latent fingerprint detection using scanning Kelvin microprobe, *Journal of Forensic Science*, 46 (2001) 1085-1092.
- [24] G. Williams, H. N. McMurray, The mechanism of group (I) chloride initiated filiform corrosion on iron, *Electrochemistry Communications*, 5 (2003) 871-877.

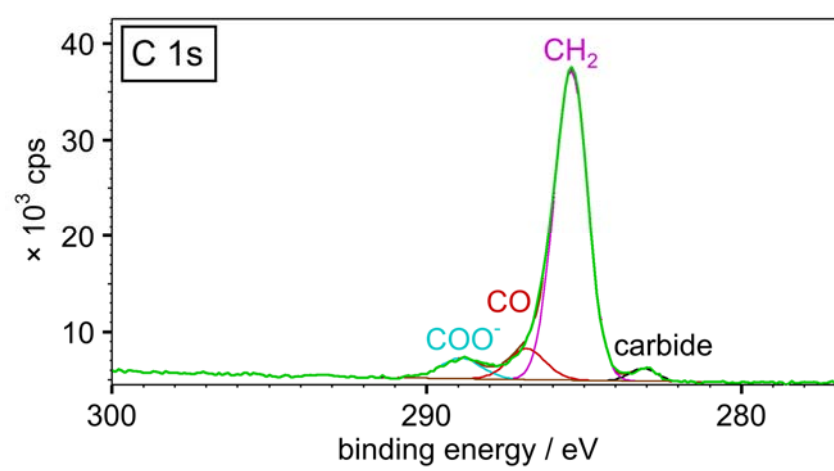
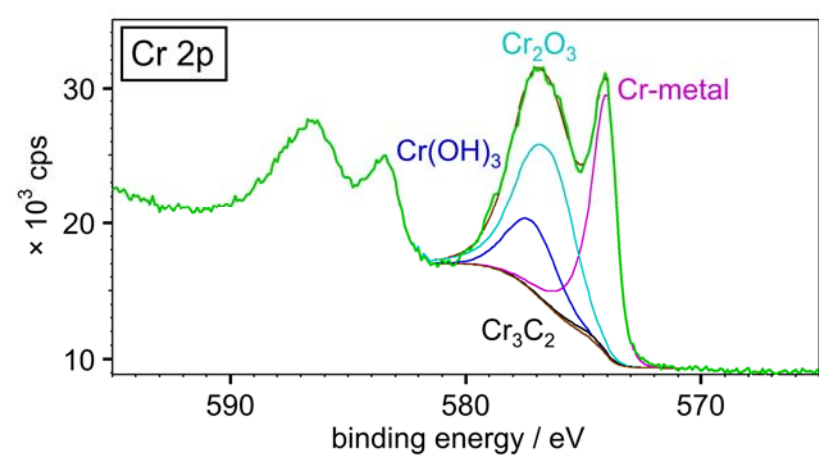
- [25] E. Zumelu, F. Rull, A.A. Boettcher, Characterization and micro- and ultra-structural analysis of PET-based Co-rolled composite electrolytic chromium coated steel (ECCS), *Journal of Materials Processing Technology*, 173 (2005) 34-39.
- [26] M. Pourbaix, N. de Zoubov, *Atlas of Electrochemical Equilibria in Aqueous Solution*, Pergamon Press, Oxford New York, 1966.
- [27] R. J. Holness, G. Williams, D. A. Worsley, Polyaniline inhibition of corrosion-driven coating cathodic delamination on iron, *Journal of the Electrochemical Society*, 152 (2005) B73-B85.
- [28] A. Leng, H. Streckel, M. Stratmann, The delamination of polymeric coatings from steel. Part 2: First stage of delamination effect of type and concentration of cations on delamination, chemical analysis of the interface, *Corrosion Science*, 41 (1999) 579-597.
- [29] M. Stratmann, R. Feser, A. Leng, Corrosion protection by organic films, *Electrochimica Acta*, 39 (1994) 1207-1214.
- [30] A. Leng, H. Streckel, M. Stratmann, The delamination of polymeric coatings from steel. Part 3: Effect of the oxygen partial pressure on the delamination reaction and current distribution at then metal/polymer interface. 41 (1999) 599-620.
- [31] N. Fink, N., B. Wilson, G. Grundmeier, Formation of ultra-thin amorphous conversion films on zinc alloy coatings. Part 1. Composition and reactivity of native oxides on ZnAl (0.05%) coatings, *Electrochimica Acta*, 51 (2006) 2956-2963.
- [32] G. M. Hoch, in *Localized Corrosion*, R. W. Staehle, B. F. Brown, J. Kruger, and A. Agrawal, (Eds), NACE International, Houston, TX 134, 1974, p. 134.

[33] W. Funke, Toward a unified view of the mechanism responsible for paint defects by metallic corrosion, *Industrial and Engineering Chemistry Product Research and Development*, 24, (1985) 343-347.

[34] T. M. Watson, A. J. Coleman, G. Williams, H. N. McMurray, The effect of oxygen partial pressure on the filiform corrosion of organic coated iron, *Corrosion Science*, 89 (2014) 46-58.

[35] M. K. Harun, J. Marsh, S.B. Lyon, The effect of surface modification on the cathodic disbondment rate of epoxy and alkyd coatings, *Progress in Organic Coatings*, 54 (2005) 317-321.

Figures



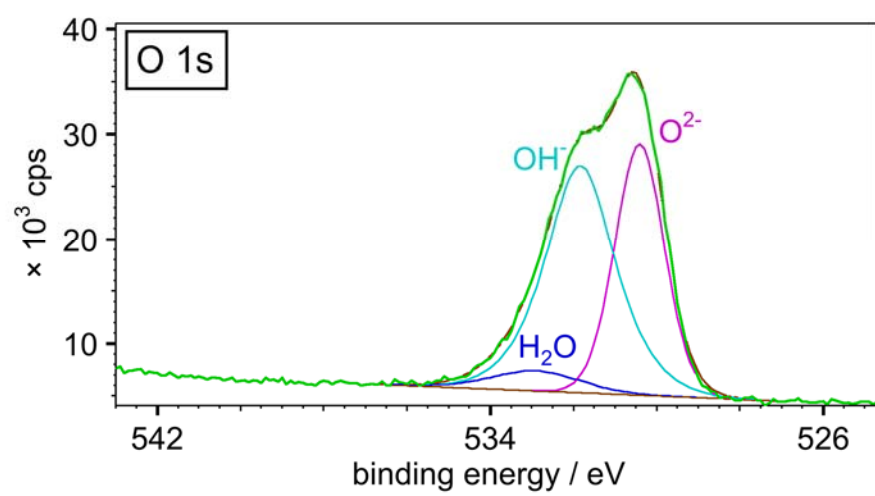


Figure 1: Example of XPS spectra from the outermost surface of sample with fitted curves for i.) metallic Cr, ii.) Cr carbides and iii.) Cr oxides [5].

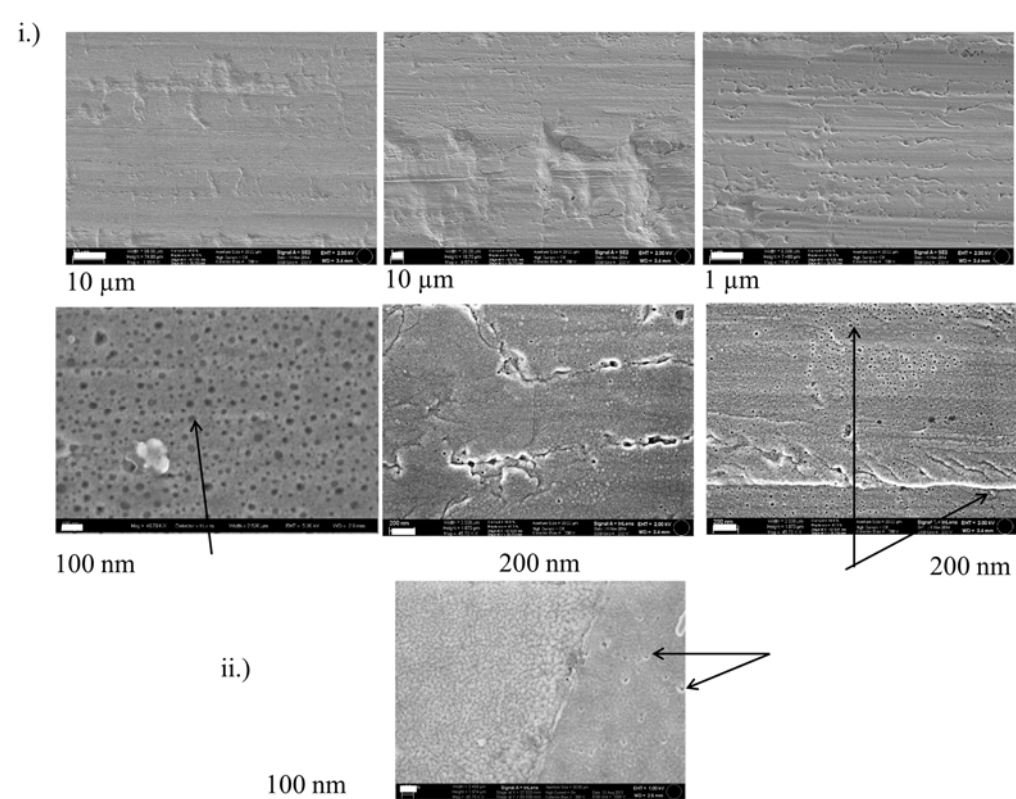


Figure 2: SEM images (InLens detector) at increasing magnification showing the i.) Cr³⁺ based coating ii.) Cr⁶⁺ based coating (ECCS). Arrows indicate areas at which hydrogen bubbles are suggested to form.

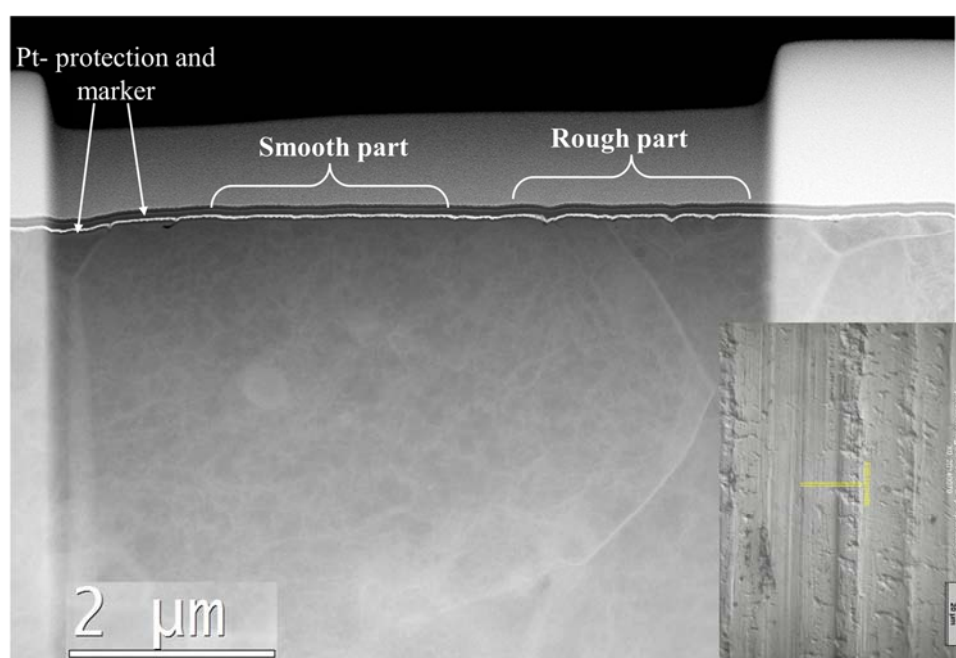


Figure 3: LIM image showing position from which sample is cut (inset), and overview of FIB-TEM image, where the white layer is platinum and shows the location of the original substrate/air interface.

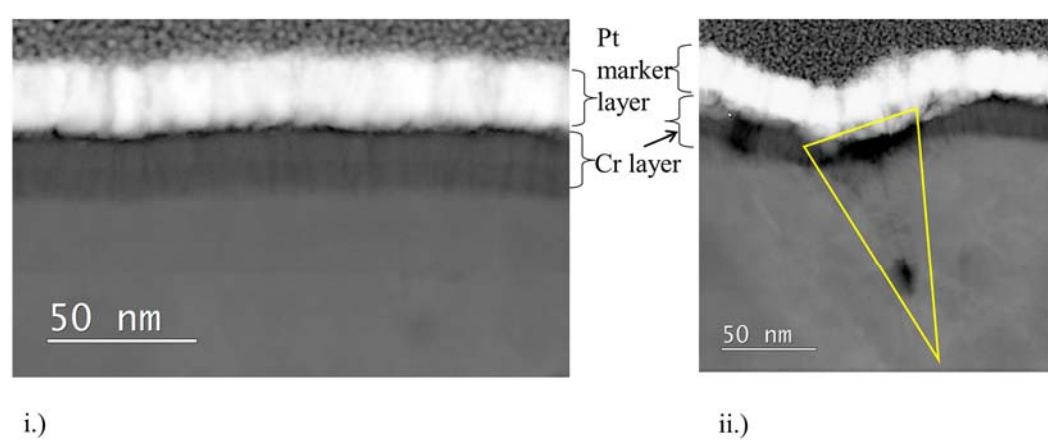


Figure 4: Enlargements of Figure 3 on the i.) smooth part ii.) rough part.

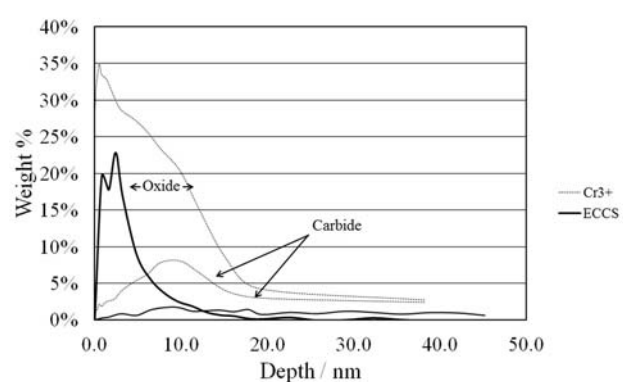
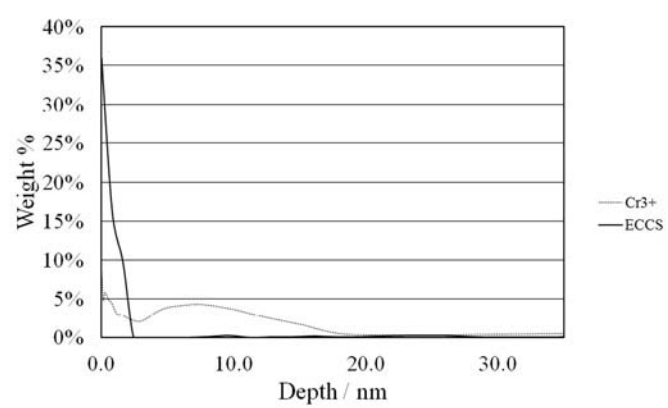
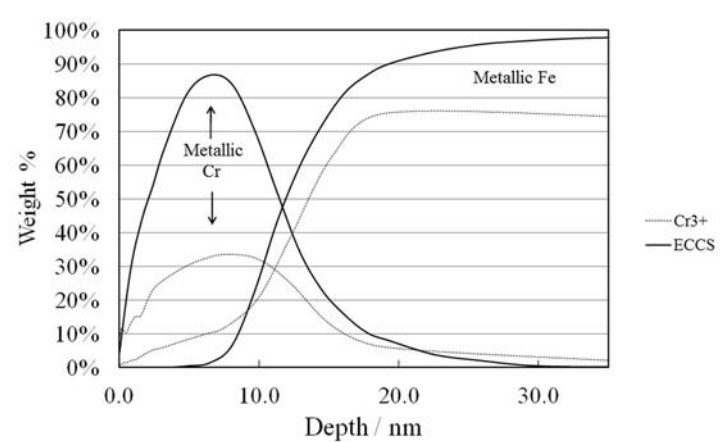


Figure 5: XPS spectra measured for Cr³⁺ coated blackplate and ECCS and deconvoluted into respective species, alternated with a short sputtering for i.) Cr and Fe metal, ii.) Cr hydroxide and iii.) Cr carbide and oxide.

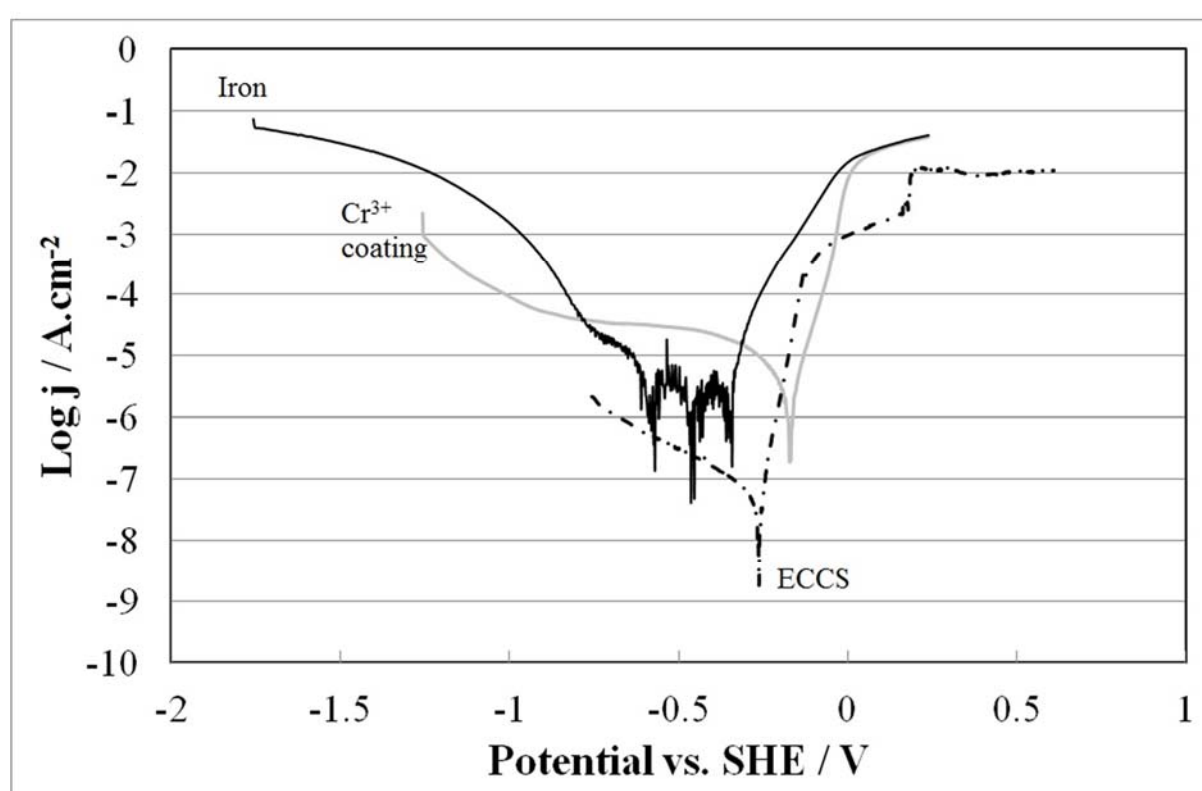


Figure 6: Current density as a function of potential for pure iron, ECCS and Cr³⁺ coated blackplate measured in aerated 0.6 mol.dm⁻³ NaCl. Potential sweep rate 0.1667 x10⁻³ Vs⁻¹.

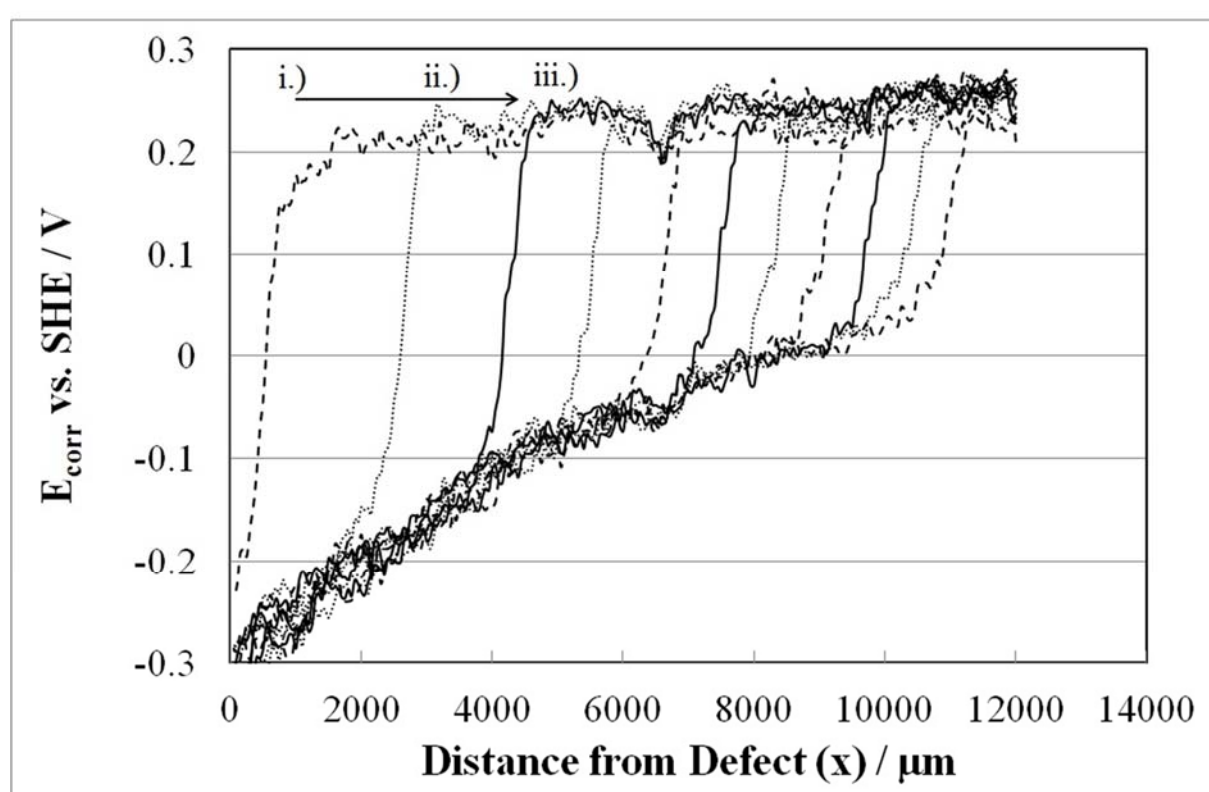


Figure 7: SKP derived E_{corr} vs. distance (x) profiles for pure iron overcoated with a 30 μm PVB film, held in air at 95% R.H., where corrosion was initiated using 0.86 mol.dm⁻³ NaCl (aq.) applied to a penetrative coating defect. Time key i.) 60 mins ii.) 120 mins iii.) 180 mins and one hour intervals thereafter.

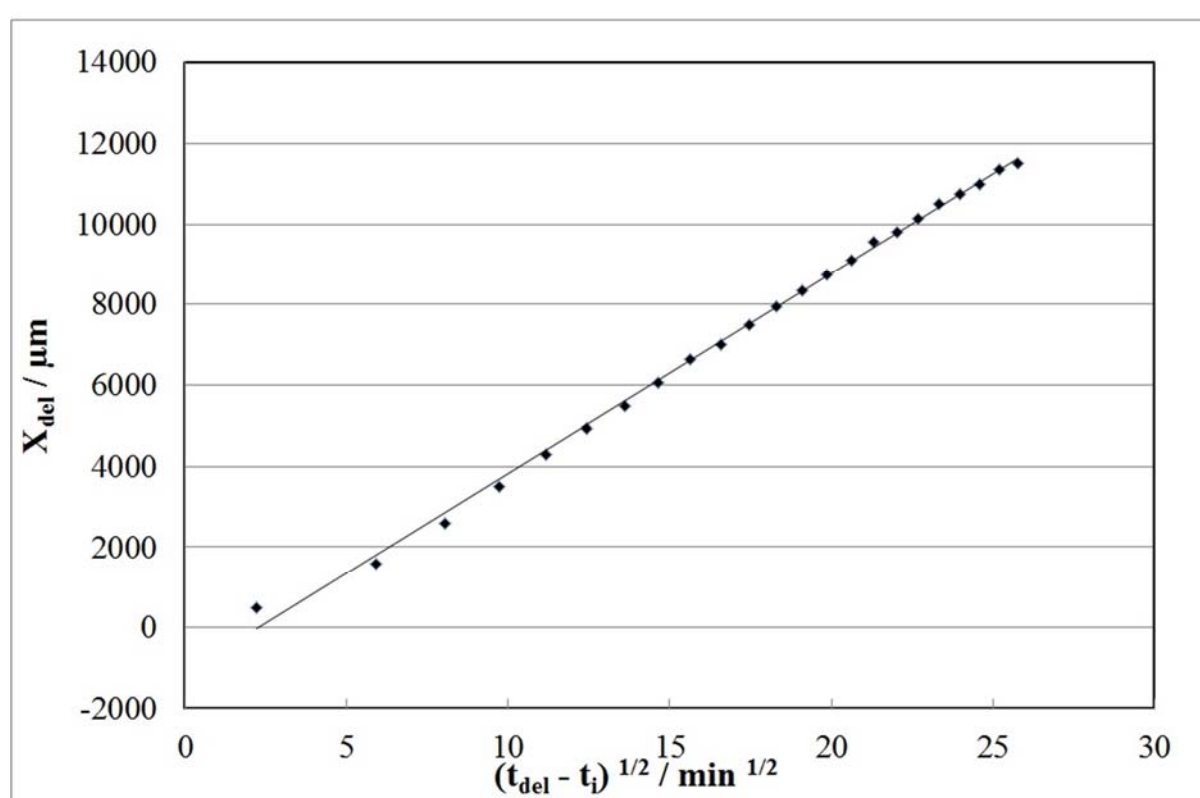


Figure 8: Plots of delamination distance (x_{del}) vs. $t^{1/2}$ obtained for a pure iron sample overcoated with a 30 μm PVB film where corrosion was initiated using a 0.86 $\text{mol}\cdot\text{dm}^{-3}$ NaCl electrolyte.

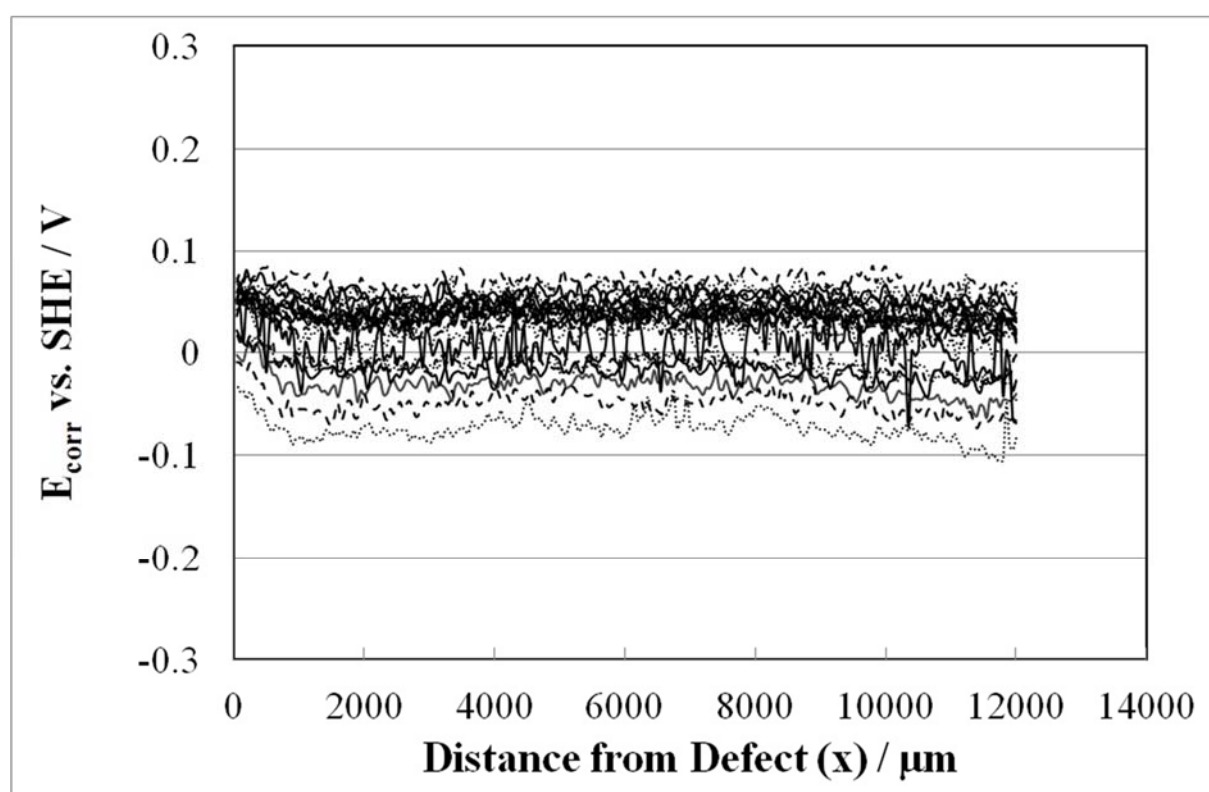


Figure 9: SKP derived E_{corr} vs. distance (x) profiles for a ECCS overcoated with a 30 μm PVB film, held in air at 95% R.H., where corrosion was initiated using 0.86 mol.dm⁻³ NaCl (aq.) applied to a penetrative coating defect.

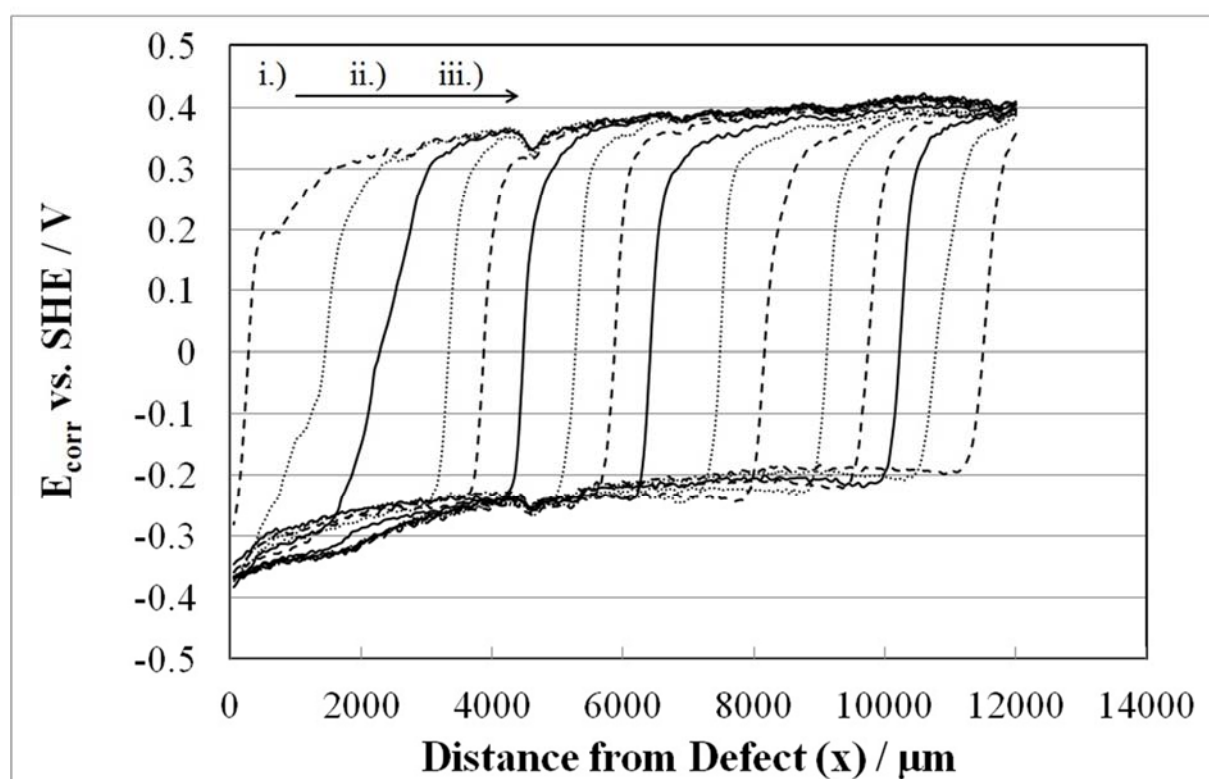


Figure 10: SKP derived E_{corr} vs. distance (x) profiles for a Cr^{3+} coated blackplate sample overcoated with a 30 μm PVB film, held in air at 95% R.H., where corrosion was initiated using 0.86 $\text{mol}\cdot\text{dm}^{-3}$ NaCl (aq.) applied to a penetrative coating defect. Time key i.) 660 mins ii.) 780 mins iii.) 900 mins and two hour intervals thereafter.

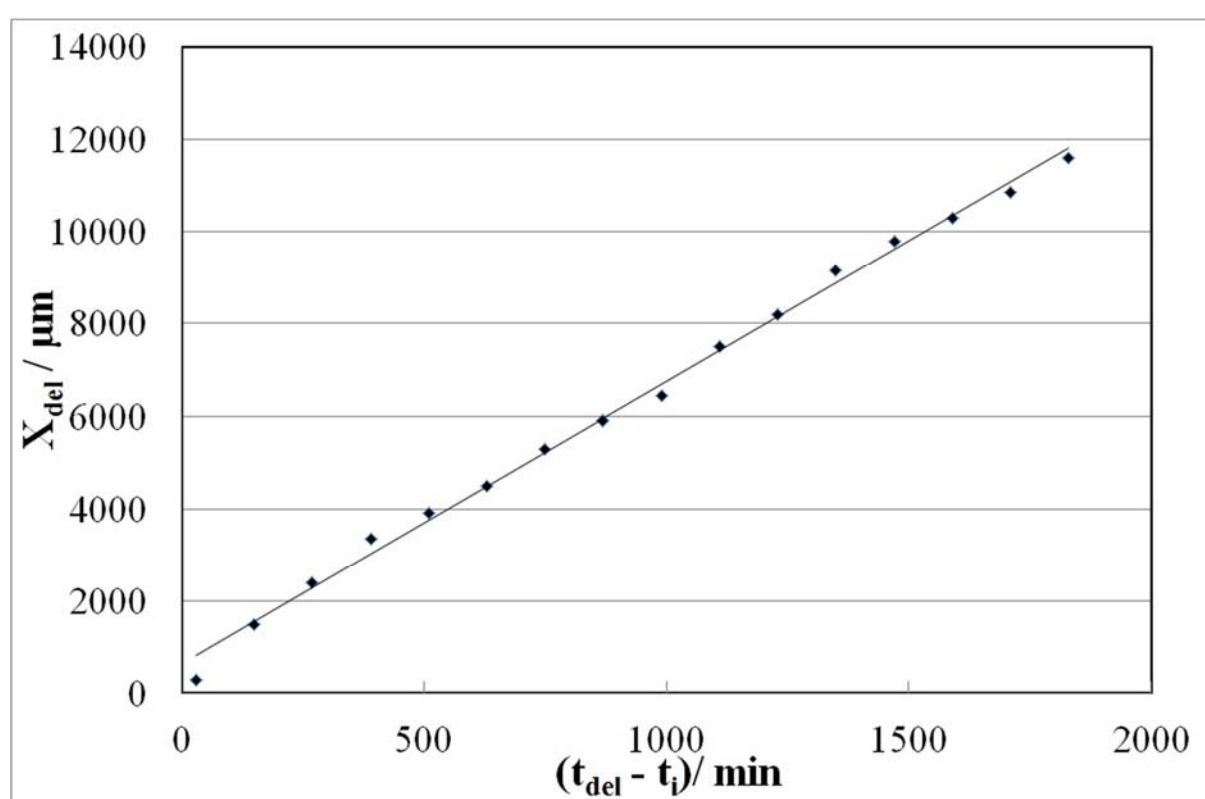


Figure 11: Plots of delamination distance (x_{del}) vs. t obtained for Cr^{3+} coated blackplate sample overcoated with a $30 \mu\text{m}$ PVB film where corrosion was initiated using a 0.86 mol.dm^{-3} NaCl electrolyte.

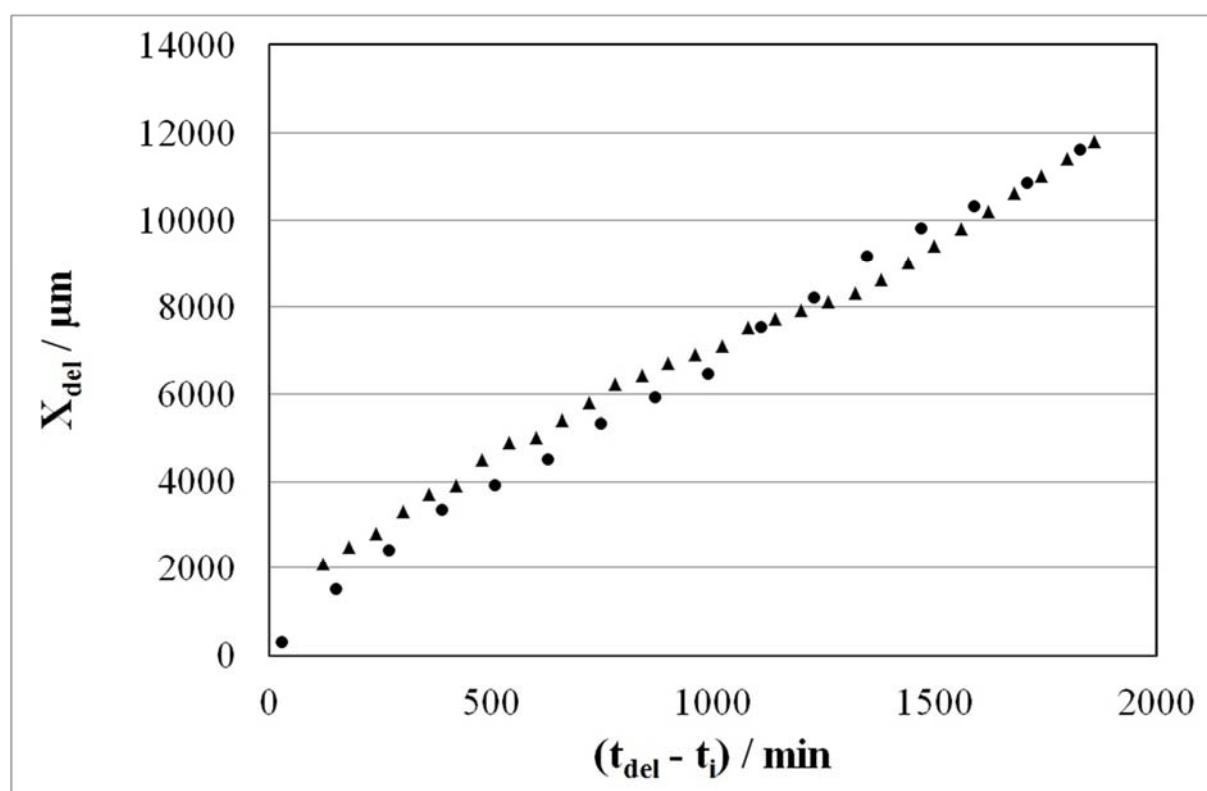


Figure 12: Plots of delamination distance (x_{del}) vs. t obtained for Cr^{3+} coated blackplate sample overcoated with a $30 \mu\text{m}$ PVB film where corrosion was initiated using a 0.86 mol.dm^{-3} ● NaCl and ▲ CsCl electrolyte.

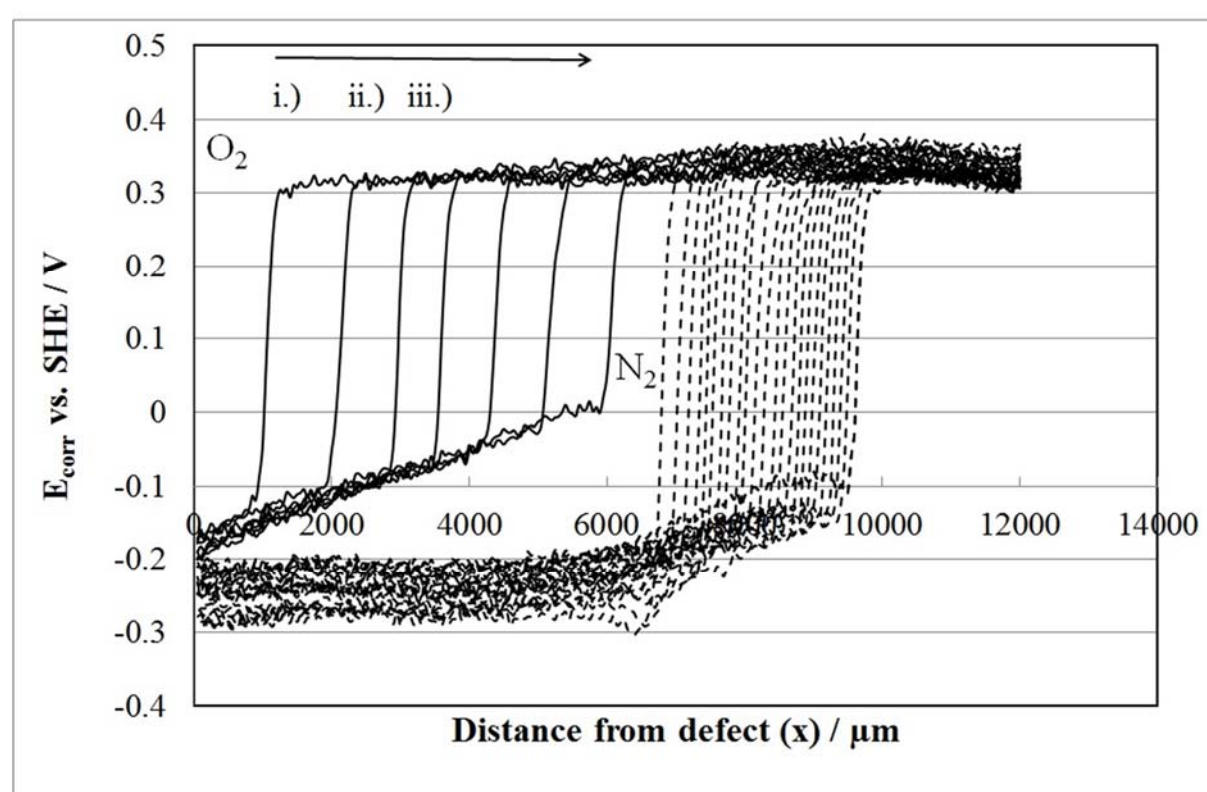


Figure 13: SKP derived E_{corr} vs. distance (x) profiles for a Cr^{3+} coated blackplate sample overcoated with a $30\ \mu\text{m}$ PVB film, held at 95% R.H., where corrosion was initiated using $0.86\ \text{mol}\cdot\text{dm}^{-3}$ NaCl (aq.) applied to a penetrative coating defect, in the presence of O_2 prior to propagation in a deaerated atmosphere. Time key i.) 440 mins ii.) 600 mins iii.) 660 mins and one hour intervals thereafter.

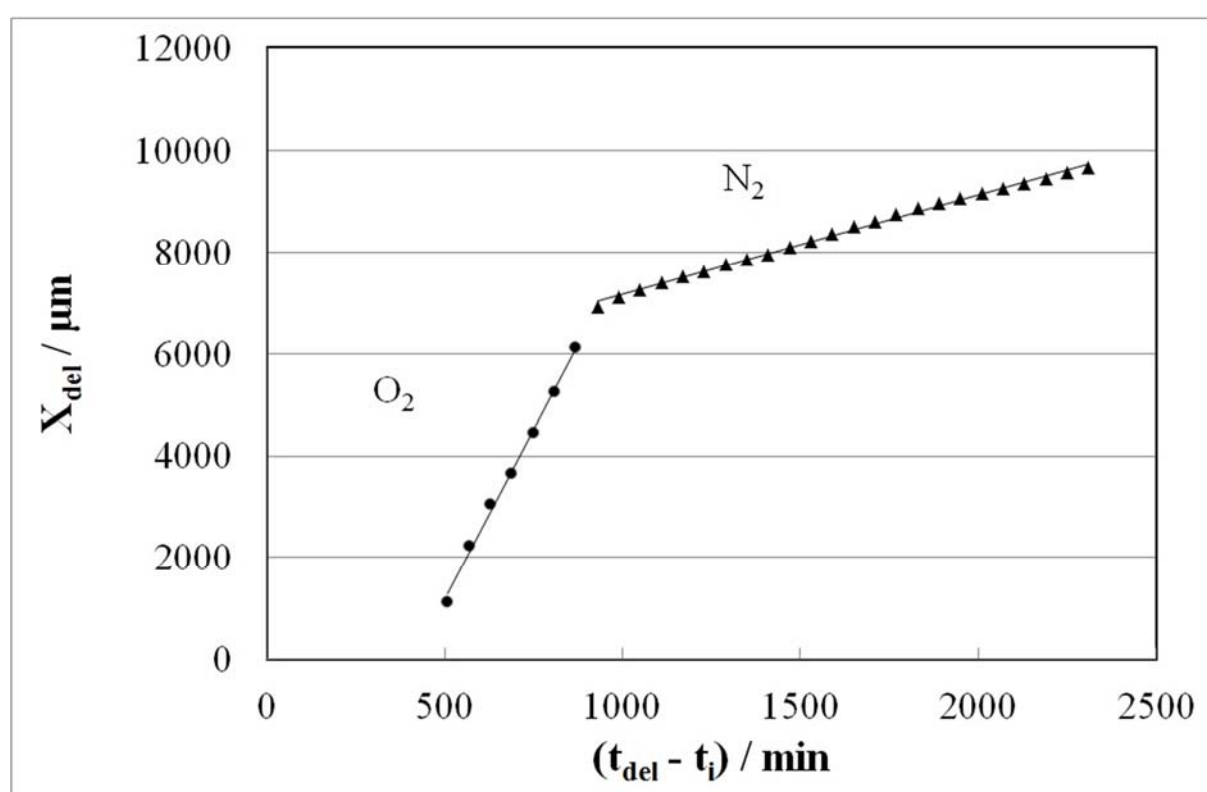


Figure 14: Plots of delamination distance (x_{del}) vs. t obtained for Cr^{3+} coated blackplate sample overcoated with a 30 μm PVB film whereby corrosion was initiated using a 0.86 $\text{mol}\cdot\text{dm}^{-3}$ NaCl electrolyte in the presence of O_2 (\bullet) prior to propagated in a deaerated atmosphere (\blacktriangle).

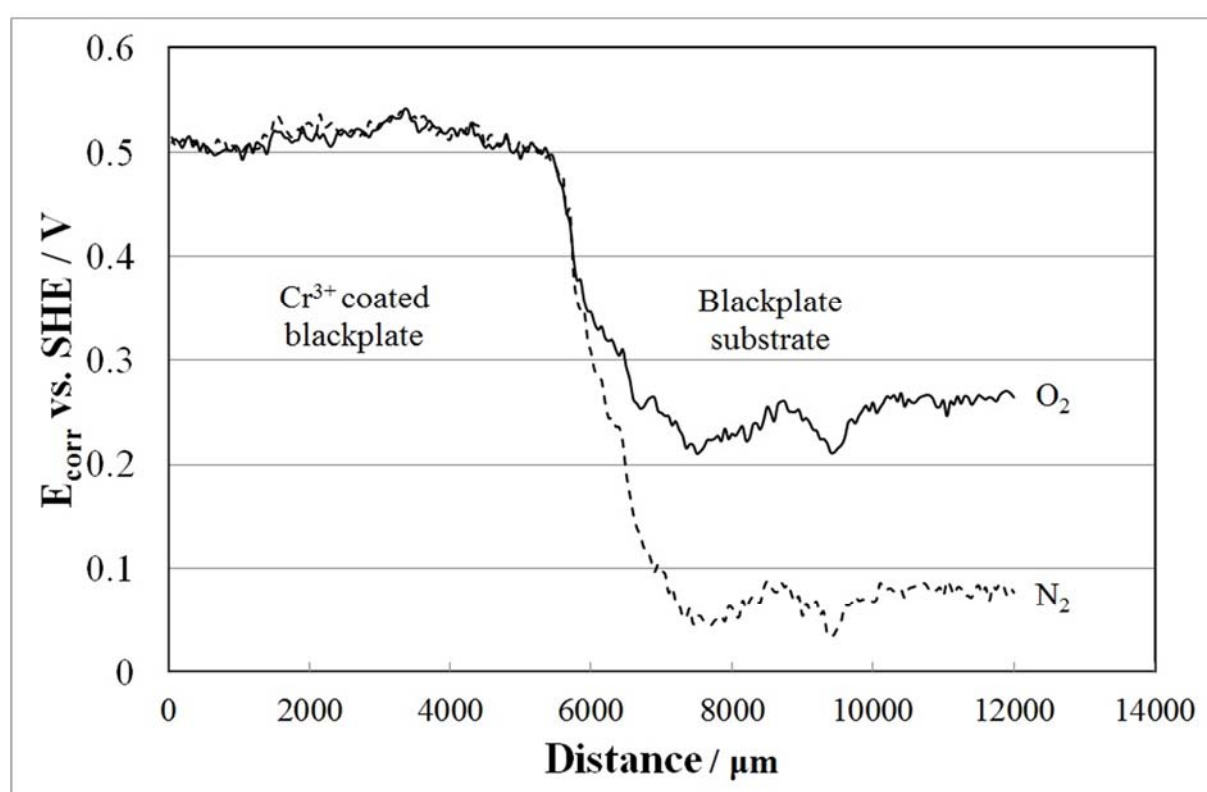


Figure 15: SKP derived E_{corr} vs. distance (x) profile obtained for both Cr^{3+} coated blackplate and blackplate in both the presence and absence of O_2 .

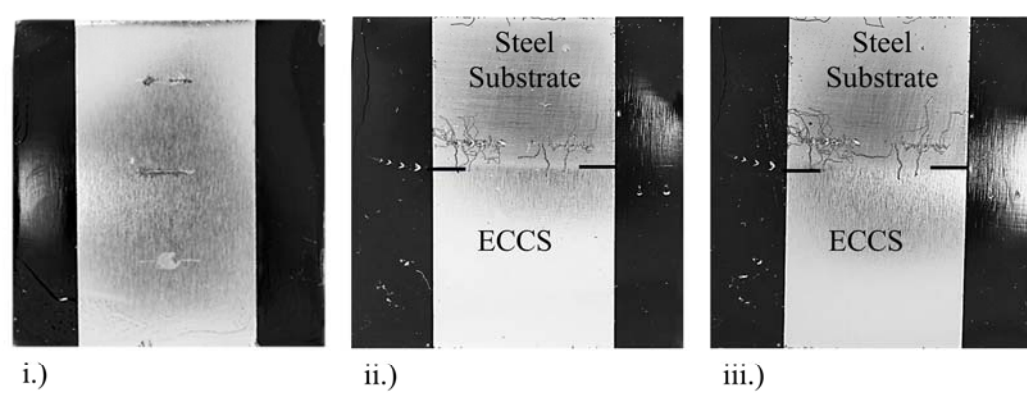


Figure 16: Photographs of samples showing that i.) FFC could not be initiated on ECCS and ii.) FFC propagated into ECCS 3 weeks after initiation on a steel substrate and iii.) FFC propagated into ECCS 5 weeks after initiation on a steel substrate, using 0.0025 M FeCl₂. Black lines indicate the border between coated and uncoated region.

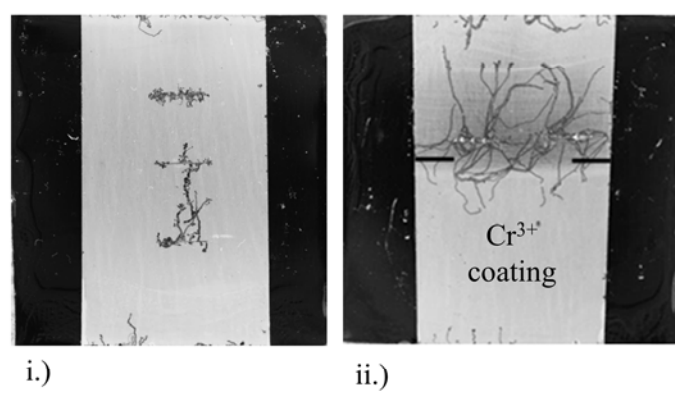


Figure 17: Photographs of samples taken after 5 weeks showing that i.) FFC could be initiated on Cr³⁺ coated steel and ii.) FFC propagated into Cr³⁺ coated steel when initiated on a steel substrate. Black lines indicate the border between coated and uncoated region.

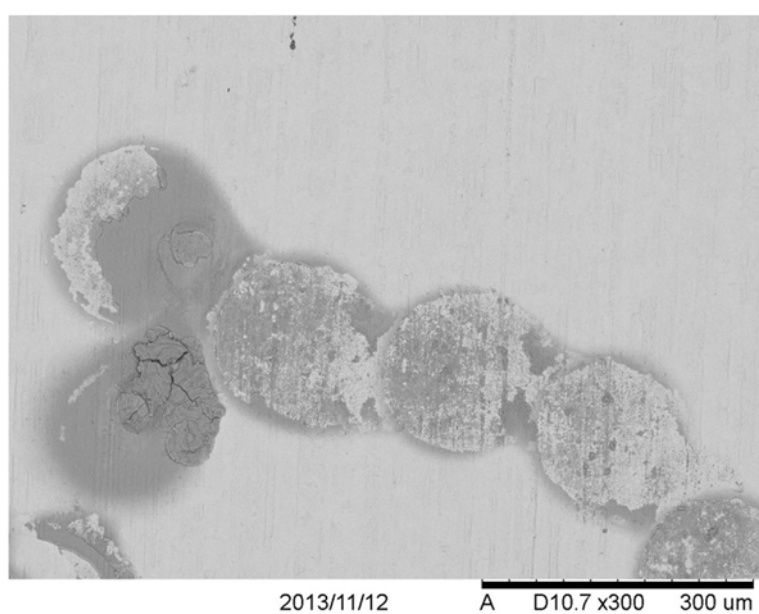


Figure 18: SEM images of FFC initiated using 0.0025 M FeCl₂ on Cr³⁺ coated blackplate.

Propagation direction is from right to left. Scale bar 300 μm.

Tables

Table I. Free Corrosion Potential of pure iron, ECCS and Cr³⁺ coated steel in 0.1M HCl at 20°C. The confidence limits (errors) shown correspond to \pm one unit of standard deviation on the mean, on the basis of three repeat measurements.

Material	E_{corr} (V vs. SHE)
Pure Iron	-0.320 \pm 0.0081
ECCS	-0.319 \pm 0.0015
Cr ³⁺ coated steel	-0.322 \pm 0.0071